335

# Investigation on the seismic performance of T-shaped column joints

Changhong Chen[*1], He Gong[1], Yao Yao[1], Ying Huang[**2] and Leon M. Keer[3]

[1]*School of Mechanics, Civil Engineering and Architecture, Northwestern Polytechnical University, Xi'an 710012, China*
[2]*School of Civil Engineering, Xi'an University of Architecture and Technology, Xi'an 710055, China*
[3]*Civil and Environmental Engineering, Northwestern University, Evanston, IL 60286, USA*

**Abstract.** More and more special-shaped structural systems have been widely used in various industrial and civil buildings in order to satisfy the new structural system and the increasing demand for architectural beauty. With the popularity of the special-shaped structure system, its seismic performance and damage form have also attracted extensive attention. In the current research, an experimental analysis of six groups of (2/3 scale) T-shaped column joints was conducted to investigate the seismic performance of T-shaped column joints. Effects of the beam cross section, transverse stirrup ratio and axial compression ratio on bearing capacity and energy dissipation capacity of column joints were obtained. The crack pattern of T-shaped column joints under low cyclic load was presented and showed a reversed "K" mode. According to the crack configurations, a tensile-shear failure model to determine the shear bearing capacity and crack propagation mechanisms is developed.

**Keywords:** T-shaped column joint; experimental analysis; crack configuration; tensile-shear model; shear resistance

## 1. Introduction

The T-shaped, I-shaped, and Z-shaped column, which have been widely used in the internal structure of buildings to replace the conventional rectangular column, are beneficial for the architecture and have broad prospects in modern housing systems. With the popularization of the special-shaped column structure, the structural performance has attracted attention of researchers. Since the 1960s, the performance of joints has been investigated as an essential subject in the seismic resistance of frames (Hanson and Conner 1967). The beam-column joints are sensitive to shear failure, and one of the major reasons for destruction in earthquakes is insufficient capacity of beam-column joints. Joint shear failure generally results in the non-ductile failure of structures (Ghobarah 2002, Wang *et al.* 2012) and can cause serious damage to the entire structure. In order to avoid collision between the rebar of the beam and column, the longitudinal reinforcements of the beam should extended into the joints after bending, which is more complicated than that in traditional rectangular joints. Therefore, it is crucial to investigate the mechanical behavior and failure models of the specially shaped beam-column joints in earthquakes.

Cao *et al.* (1995) made a test of fifteen reinforced concrete T-shaped columns under cyclic loading, where the strength, rigidity and ductility of T-shaped column in three different horizontal directions were analyzed experimentally and the applicability of the plane assumption and restoring

force model were discussed. Dundar and Sahin (1993) proposed an approach to predict the ultimate bearing capacity and strength of arbitrary cross section columns under biaxial bending and uniaxial compression. Kim and LaFave (2009) developed a shear deformation model for joints based on an experimental analysis. Wang *et al.* (2012) idealized the reinforced concrete (RC) in the joint panel as a homogenous material and proposed a shear strength model for traditional (RC) joints subjected to seismic loading. The hysteretic response and energy dissipation capacity of 10 L-shaped columns under seismic load were investigated by Pham and Li (2015), where the research showed that the axial forces have negligible effect on shear strength of joint. Barbhuiya (2015) has been tested on three types of beam column connections to indicate the existence of size effect. To further explore the seismic behavior and failure mode of RC beam column joints, a simplified analytical model is put forward by Bossio (2015) and theoretical simulations are performed. Behnam (2017) investigated the seismic behaviour of the Exterior RC wide beam-column connections, and analyses the damage of the joint core in the case of different beam width ratios. The seismic performance of the fabricated confined concrete beam-to-column connection with end-plates is tested by Li (2018), and the formula of flexural bearing capacity based on the theory of concentrated plastic zone is proposed. Besides, a large number of experimental tests and numerical simulations for traditional rectangular joints have been conducted (Hanson and Conner 1967, Scott 1992, Hwang and Lee 2000, Bakir and Boduroğlu 2002, Ghobarah *et al.* 2002, Hwang *et al.* 2005, Kim and LaFave 2007, Tsonos 2007, Wong and Kuang 2008, Lee *et al.* 2009, LaFave and Kim 2011, Park and Mosalam 2012, Unal and Burak 2012, *Wang et al.* 2012, Masi *et al.* 2013, Jeon *et al.* 2014, Chen *et al.* 2016, Chen *et al.* 2016, Ricci *et al.* 2016), and some

---

∗Corresponding author, Associate Professor
 E-mail: changhong.chen@nwpu.edu.cn
∗∗Corresponding author, Associate Professor
 E-mail: xiancch@gmail.com

crucial influence parameters for joint shear-resistance capacity were studied (Scott 1992, Hwang and Lee 2000, Bakir and Boduroğlu 2002, Ghobarah *et al.* 2002, Hwang *et al.* 2005, Kim and LaFave 2007, Unal and Burak 2012,, Chen *et al.* 2016, Chen *et al.* 2016), such as column size, column axial load. New methods to predict shear-resistance capacity were proposed (Ghobarah *et al.* 2002, Hwang *et al.* 2000, Chen *et al.* 2016, Chen *et al.* 2016, Bakir and Boduroğlu 2002, Lee *et al.* 2009, Park and Mosalam 2012).

Despite extensive studies that have been performed on reinforced concrete T-shaped columns, there is not a commonly accepted method for determination of the shear strength (NZS 3101 2006, EURO code 8 2004, ACI 318 R-14 2014) and the classical joint models are not suitable to describe crack mechanism of the T-shaped column joints. The failure model for T-shaped column frame joints still requires further research. In the current research, the seismic performance of six T-shaped cross section column frame joints was tested under cyclic loads. Furthermore, the development of cracks and corresponding failure mechanisms of the joint are discussed. Based on the crack configuration in the experiment, a tensile-shear model and approach to predict the shear capacity of the T-shaped column joints has been developed.

## 2. Design of experiments
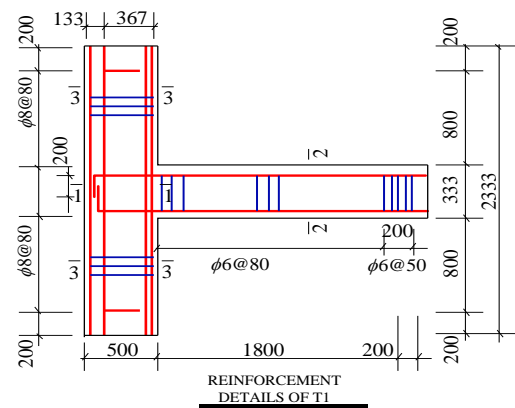
### 2.1 The parameters of specimens

The test consists of 6 (2/3 scale) T-shaped column joints specimens. The focus is on investigating the influence of beam height, axial compression ratio and transverse stirrup ratio on formation and development of cracks in the joint area, and the failure mechanism and the seismic behavior of joints. The specimens were divided into three groups, as shown in Table 1. The specimen's height is the distance between two contraflexure points (the column moment of this position is equals to zero) of the column under horizontal load. The specimen's length is the distance from the contraflexure point (the beam moment of this position is

equals to zero) of the beam under horizontal load to the edge of the column.
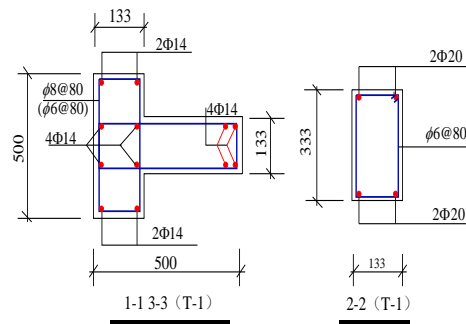
The T1 specimen is taken as a representative example to illustrate the reinforcements of specimens and construction measures, as shown in Fig. 1.

### 2.2 The material properties of specimens

The concrete grade of specimens is C30, and the longitudinal reinforcement type is HRB335, and the type of stirrup is HPB300. In order to ensure the reliability, the performance indexes were adopted from measured



(a) Reinforcement layout of T1 (Profile)



(b) Reinforcement layout of T1 (Section view)

Fig. 1 Reinforcement of specimen

Table 1 The parameters and classifications of specimens

| Groups | | First group | | | Second group | | | Third group | |
|---|---|---|---|---|---|---|---|---|---|
| Specimens | | T1 | T2 | T3 | T4 | T2 | T5 | T2 | T6 |
| Beam section | | 133×133 | 133×400 | 133×500 | 133×400 | 133×400 | 133×400 | 133×400 | 133×400 |
| Column section | | $h_c=b_f=500, h_f=b_c=133$ | | | | | | | |
| $h_c/h_c$ | | 0.667 | 0.8 | 1.0 | 0.8 | 0.8 | 0.8 | 0.8 | 0.8 |
| Rebar in beam | Longitudinal reinforcements | 4Φ20 | 4Φ20 | 4Φ20 | 4Φ20 | 4Φ20 | 4Φ20 | 4Φ20 | 4Φ20 |
| | Transverse reinforcements | φ6@ | φ6@ | φ6@ | φ6@ | φ6@ | φ6@ | φ6@ | φ6@ |
| Rebar in column | Longitudinal reinforcements | 12Φ14 | 12Φ14 | 12Φ14 | 12Φ14 | 12Φ14 | 12Φ14 | 12Φ14 | 12Φ14 |
| | Transverse reinforcements | φ8@80 | φ8@80 | φ8@80 | φ8@80 | φ8@80 | φ8@80 | φ8@80 | φ8@80 |
| Reinforcements of core field | | φ6@80 | φ6@80 | φ6@80 | φ6@80 | φ6@80 | 0 | φ6@80 | φ6@80 |
| $\rho_{sv}$ | | 0.87% | 0.87% | 0.87% | 0.87% | 0.87% | 0 | 0.87% | 1.53% |
| Axial compression ratio | | 0.12 | 0.12 | 0.12 | 0.5 | 0.12 | 0.12 | 0.12 | 0.12 |

Table 2 The parameters of concrete specimens

| Number of specimens | Cube crushing strength $f_{cu}$ (MPa) | Prismatic compressive strength $f_c$ (MPa) | Tensile strength $f_t$ (MPa) | Elastic modulus $E_c$ ($\times 10^4$ MPa) |
|---|---|---|---|---|
| T1 | 36.4 | 12.12 | 2.86 | 3.4 |
| T2 | 39.6 | 14.68 | 3.02 | 3.12 |
| T3 | 35.3 | 11.7 | 2.80 | 3.19 |
| T4 | 36.5 | 12.2 | 2.86 | 3.5 |
| T5 | 35.6 | 11.48 | 2.81 | 3.20 |
| T6 | 35.0 | 11.00 | 2.78 | 3.18 |

Table 3 The parameters of reinforcements

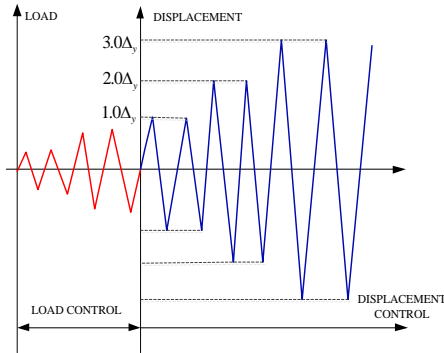| Reinforcement grade | Diameter (mm) | Yield strength $f_t$ (MPa) | Ultimate strength $f_u$ (MPa) | Elastic modulus $E_c$ ($\times 10^5$ MPa) |
|---|---|---|---|---|
| HRB335 | 20 | 389.9 | 568.2 | 2.06 |
| HRB335 | 14 | 350.9 | 535.9 | 2.08 |
| HPB300 | 8 | 148.2 | 465.53 | 2.10 |
| HPB300 | 6 | 146.7 | 456.17 | 2.09 |



Fig. 2 Loading method of specimens

experimental data. Three concrete samples were reserved for each joint, and the maintenance condition was consistent with specimens. Three samples of reinforcements were selected randomly for each type, which were regarded as performance indexes of reinforcements. Experiments on joint material properties were carried out simultaneously. The average values of experimental date are taken as the performance indexes of the specimens. The experimental parameters of the concrete specimens and reinforcements are shown in Tables 2-3, respectively.

### 2.3 Loading system

In this research, a pseudo static method is employed to simulate the seismic action, while a loading method based load and displacement control was applied. To ensure axial compression of column, the loading point is settled at the center of top surface of the T-shaped column. This load was maintained constant in the subsequent process (constant axial pressure). Then, cyclic loading was applied at the end of beam by using the tension and compression jack. Load control was applied before the specimen yielded, and displacement control was adopted after the specimens yielded. Failure is regarded as when the specimens reach
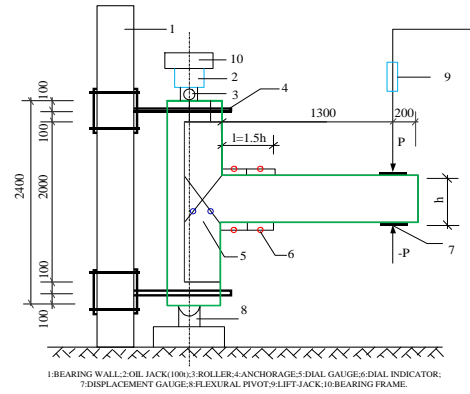


1:BEARING WALL;2:OIL JACK(100t);3:ROLLER;4:ANCHORAGE;5:DIAL GAUGE;6:DIAL INDICATOR; 7:DISPLACEMENT GAUGE;8:FLEXURAL PIVOT;9:LIFT-JACK;10:BEARING FRAME.

Fig. 3 Loading devices for joint specimens

Table 4 Experimental results

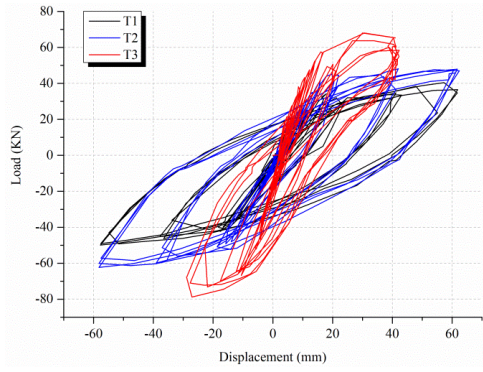| Number | Loading direction | Initial cracking shear $V_j$ Initial load $F_{cr}$ | Initial cracking shear $V_j$ | Yield load $F_y$ (KN) | Ultimate load $F_u$ (KN) | Failure form |
|---|---|---|---|---|---|---|
| T1 | + | 13 | 75.5 | 34.3 | 40.40 | Beam end failure |
| | - | 35 | | 42.14 | 49.90 | |
| T2 | + | 35 | 64.4 | 43.93 | 50.00 | Beam end failure |
| | - | 35 | | 49.19 | 62.13 | |
| T3 | + | 45 | 52.6 | 57.44 | 61.39 | Beam end failure |
| | - | 45 | | 66.2 | 76.47 | |
| T4 | + | 40 | 72.7 | 43.71 | 50.20 | Beam end failure |
| | - | 45 | | 50.59 | 58.65 | |
| T5 | + | 35 | 61.7 | 42.52 | 48.14 | Beam end failure |
| | - | 40 | | 50.72 | 54.72 | |
| T6 | + | 35 | 69.9 | 40.72 | 42.33 | Beam end failure |
| | - | 45 | | 54.77 | 67.66 | |

*Note: the vertical loading direction is "+".

the maximum bearing capacity and down to 80%-85%. The specimen's loading system and loading device are shown in Fig. 2 and Fig. 3, respectively.
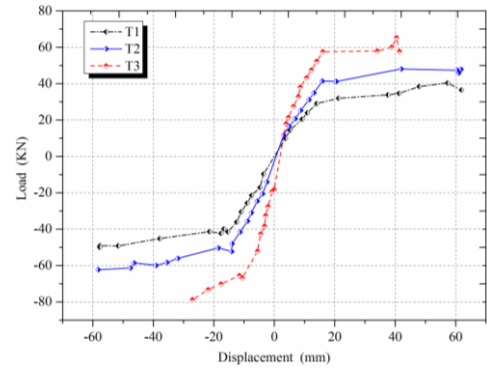
## 3. Analysis of experimental results

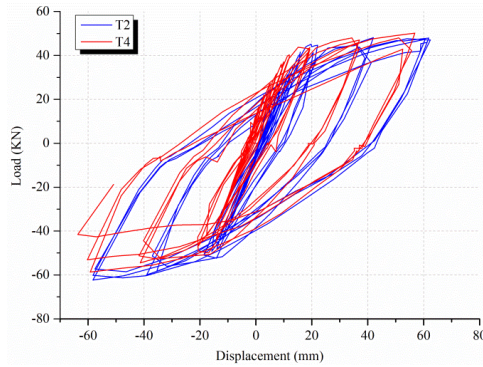### 3.1 Analysis of bearing capacity

All the specimens exhibit ideal beam hinge failure under cyclic loading, where experimental results are shown in Table 4. The yield bearing capacity and ultimate bearing capacity of T1, T2 and T3 increases gradually and proves that the bearing capacity of the T-shaped column joints has improved significantly with increasing beam height. Additionally, the initial crack load of joints has emerged downward, because the ductility is reduced with larger beam height, and the ratio of reinforcement remains invariant. Experimental data of T2 and T4 shows that the initial crack shear improves significantly and there is
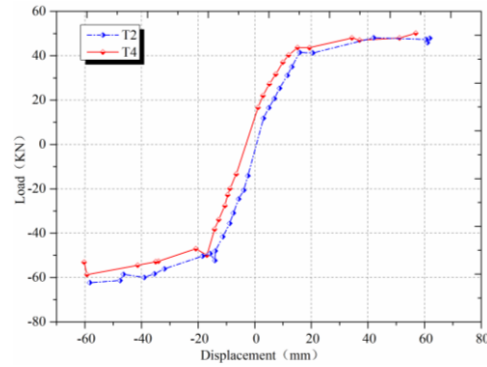
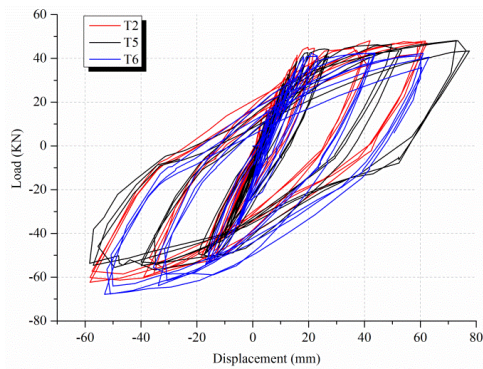(a) Comparisons of load-displacement hysteretic curves of T1, T2, T3

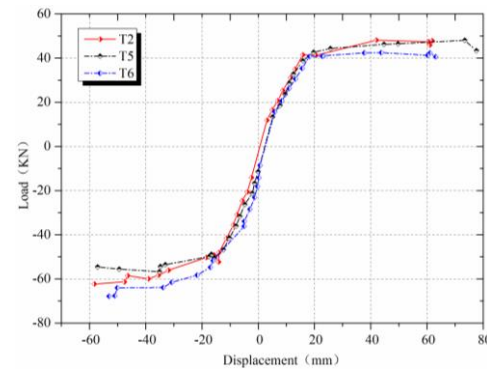(b) Comparisons of skeleton curves of T1, T2, T3

(c) Comparisons of load-displacement hysteretic curves of T2, T4

(d) Comparisons of skeleton curves of T2, T4

(e) Comparisons of load-displacement hysteretic curves of T2, T5, T6

(f) Comparisons of skeleton curves of T2, T5, T6

Fig. 4 Comparisons of load-displacement hysteretic curves and comparisons of skeleton curves

appearance of a crack delay with the increase of the axial compression ratio; nevertheless the yield bearing capacity and ultimate bearing capacity have no obvious change. By contrast with experimental results of T2, T5 and T6, the improvement of transverse stirrup ratio in the core area of beam-column joints will increase the crack shear, and the yield bearing capacity and ultimate bearing capacity still have no obvious change. Based on the beam hinge failure mechanism, the size of beam section has profound impact to bearing capacity of T-shaped beam-column joints, while the effects of axial compression ratio and transverse stirrup ratio can be neglected.

### 3.2 Hysteretic curve

Comparisons of the load-displacement hysteretic curves

and skeleton curves of T1, T2 and T3 are shown in Figs. 4 (a)-(b). With increasing of the beam section height, the flexural rigidity ratio of column to beam decreases continuously, and the plastic hinge position moves gradually towards the interior of the joints, which will cause lower plasticity in the joints; thus the ductility and energy dissipation capacity of T1, T2, T3 decrease gradually. It is noted that the hysteretic curve of T1 is plumper than T2 and T3, which demonstrates the pinch phenomenon.

According to Mitra and Lowes (2007), Kitayama *et al.* (1988), the bond index of reinforcement in beam is defined as

$$\mu = \frac{f_y b_d}{2h_c \sqrt{f_c}} \tag{1}$$

where $\mu$ is the bond index; $f_y$ is the yield strength of

reinforcement in beam; $h_c$ is the height of column; $f_c$ is compressive strength of concrete.

All specimens keep identical average cohesive strength, calculated according to Eq. (1) in this experiment. Although T1, T2 and T3 maintain intact bond condition, the force transmitted by longitudinal reinforcements to the interior of the joint can be improved with increasing of the beam section height. When the applied load exceeds the ultimate bond capacity, reinforcements of the joint slips, and the longitudinal reinforcements cause bond failure to arise. However, the joint and beam have not reached the ultimate bearing capacity at this stage, as the actual bearing capacity of the structure is less than the design value. Consequently, there is an optimized combination among reinforcements, section, and bearing force. Increasing of a single performance in the structure will lead to reduction of others, and the performance of the structure is not fully optimized.

Comparisons of the load-displacement hysteretic curves and skeleton curves of T2 and T4 are shown in Figs. 4 (c)-(d). With the increase of the axial compression ratio, the load-displacement hysteretic curves of T2 and T4 are almost identical. The shear of the joints when initial cracks appear increases (the shear growth rate is 11.42%), while the lateral deformation of the frame columns is miniscule. Meanwhile, the time when diagonal cracks appear is delayed in the joint area, and it also postpones the development of a diagonal crack, and transforms the position of plastic hinge towards exterior of the joint.

The load-displacement hysteretic curves and skeleton curves of T2, T5 and T6 are compared in Figs. 4 (c)-(d). The load-displacement hysteretic curve of T6 is plumper than in the other two specimens, which manifests better ductility and energy dissipation capacity. However, T2 and T5 present pinch phenomenon, especially for T5. Both displacement ductility and energy dissipation capacity are poor. Hence, one of the keys of reinforcements in the joint area is to improve the shear strength and ductility.

Energy dissipation capacity of the structure is reflected by ductility. In this paper, the displacement ductility coefficient of the beam end $\mu_\Delta$ and the curvature ductility coefficient of plastic hinge regions $\mu_\phi$ are adopted as the indices to measure the ductility of the structure under cyclic loading, as defined in Eq. (2)

$$\mu_\Delta = \frac{\Delta_u}{\Delta_y} \quad \mu_\phi = \frac{\phi_u}{\phi_y} \tag{2}$$

where $\Delta_u$ is displacement corresponding to the ultimate bearing capacity; $\Delta_y$ is displacement corresponding to initial yield of the structure; $\phi_u$ is the maximum curvature of the plastic hinge region when structure is destroyed; and $\phi_y$ is the average curvature of the plastic hinge region corresponding to initial yield of structure.

The greater area of the load-displacement hysteresis loop and the stronger energy dissipation ability of the structure provide more favorable seismic resistance under cyclic loading. In this paper, the work ratio index proposed by Gosain *et al.* (1977) is utilized to measure the energy dissipation capacity of the T-shaped column under cyclic loading, as given in Eq. (3), and the results are shown in Table 5.

Table 5 Displacement ductility coefficient, curvature ductility factor, and work ratio index

| Number | $\Delta_y$ (mm) | $\Delta_i$ (mm) | $\mu_\Delta$ (mm) | $\phi_u$ ($\times 10^{-6}$ rad/mm) | $\phi_y$ ($\times 10^{-6}$ rad/mm) | $\mu_\phi$ | $I_w$ |
|--------|------|------|------|-------|-------|------|-------|
| T-1 | 16.67 | 61.89 | 3.7 | 11.73 | 4.11 | 6.99 | 18.97 |
| T-2 | 15.72 | 58.7 | 3.7 | 14.46 | 4.46 | 7.05 | 17.64 |
| T-3 | 16.93 | 61.39 | 3.6 | 14.72 | 4.57 | 6.94 | 16.67 |
| T-4 | 15.10 | 56.87 | 3.8 | 14.19 | 4.61 | 6.77 | 18.14 |
| T-5 | 20.48 | 72.83 | 3.6 | 11.48 | 4.5 | 6.75 | 15.62 |
| T-6 | 18.20 | 63.08 | 3.5 | 10.36 | 4.47 | 6.12 | 18.13 |

$$I_w = \sum_{i=1}^{n} \frac{F_i \Delta_i}{F_y \Delta_y} \tag{3}$$

where $n$ is cycle number; $F_y$ is the yield load; $F_i$ is the limit load of the $i$-th cycle; $\Delta_i$ is limit displacement of the $i$-th cycle.

The displacement ductility coefficient of specimens are generally identical, approximately 3.7. All the specimens with the beam hinge failure mechanism exhibit better ductility. Compared with conventional rectangular joints, the T-shaped column is closer to a fixed end beam because the beam bending stiffness is smaller than that of the column. Moreover, the failure mechanism of T-shaped column turns out to be the ideal beam hinge failure, which has negligible impact on columns and joints and is favorable to seismic design because it is easier to achieve the target of strong column and weak beam advocated by the design codes.

Compared with the conventional rectangular column ($\mu_\phi > 11$), the curvature ductility coefficient $\mu_\phi$ of T-shaped column joints in the plastic hinge zone is smaller and approximately 6~7, which shows poor ductility of the plastic hinge section of T-shaped column. The reason for this conclusion is that the beam bearing capacity in the T-shaped column structure is smaller than that of the conventional structure, therefore a small quantity of reinforcements is laid in beam of T-shaped column. With tensile failure in the tensile zone, the neutral axis moves to the compressive zone when the longitudinal reinforcement yields under tensile load, which results in increasing of the compressive stress and damage in the compressive zone of concrete. The bearing capacity is contributed by incomplete concrete crush, yielded and constitution reinforcement after the regular bearing system of the beam is damaged. When the external load continues to increase, the finite bearing reserve will be exhausted, and the beam will be completely destroyed. Hence, a small curvature ductility coefficient $\mu_\phi$ of the plastic hinge is obtained. In addition, the work ratio index showed a larger reinforcement ratio of beam (Reducing beam section is equivalent to increasing the beam volume reinforcement ratio with the same number of reinforcements), the axial compression ratio and the reinforcement ratio in the core area of joint can improve the energy dissipation capability.

*3.3 The crack analysis*

(a) Crack pattern



(b) Fracture characteristics

Fig. 5 Crack configuration and the fracture characteristics



(a) Joint of conventional    (b) Joint of T-shaped column
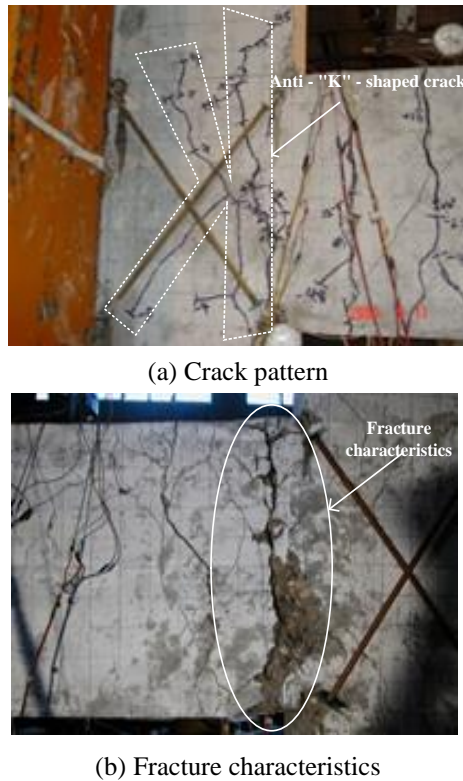rectangular column

Fig. 6 Crack configuration and the fracture characteristics

The crack processes of six specimens are generally identical from the beginning of loading to failure. With a small load, vertical cracks appeared at the beam end, while the flange and web in the core area of joint are not being cracked and are still in the elastic state, because of the small shear deformation of the core zone. With increasing of the load, cracks develop further in the beam end. Diagonal cracks at approximately 60° appear in the web of joint. Nevertheless, cracks do not appear at the flange plate in the core area of joint and longitudinal reinforcements in the beam show elastic plastic deformation. By increasing the load, the diagonal cracks in the core area of the joint keep accumulating and form a reversed "K" shape, and the number of diagonal cracks increased significantly. Moreover, a plastic hinge was formed at the beam end, and the protective layer of the concrete breaks off eventually. The maximum stress value in stirrup is only 41% of the yield strength in the flange of the core area, and web stirrups do not yield at all. The crack shape and fracture characteristics of the beam end are shown in Fig. 5.

## 4. The shear model of T-shaped joint

Typically the joint failure is divided into two types: internal bond failure and internal shear failure. If the stress transmitted from the longitudinal reinforcements to the joint is greater than the adhesion between the concrete of the joint's area and longitudinal reinforcements, slippage between longitudinal reinforcements and concrete will emerge, and lead to reduction of bearing capacity. In most of t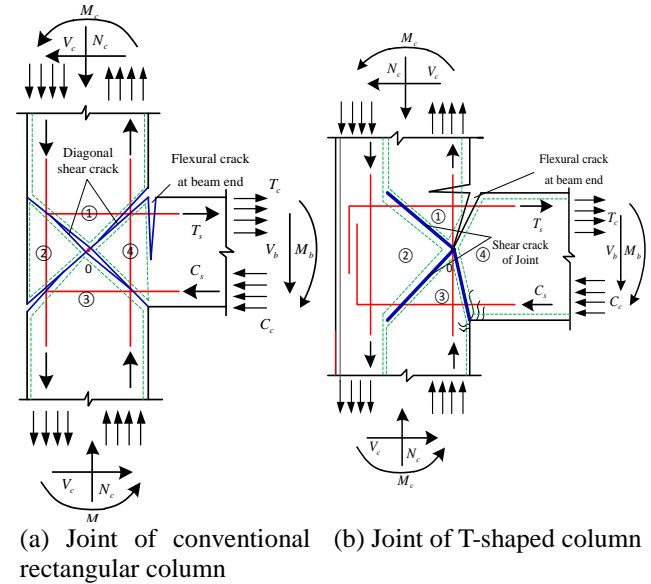he structural design codes, the bond strength failure of a beam is assumed not to be considered because there are many construction issues caused by adding the length of anchor zone. In the absence of bond strength failure, shear strength failure will occur when the stress transmitted by reinforcements to the joint is greater than the shear capacity.

The joint area between beam and column plays a significant role in the seismic resistance of structures. As an important point to the beam-column internal force distribution, joints should have not only sufficient bearing capacity, but also perfect transmission performance. The mechanical behavior and failure configuration of the conventional RC joints were studied and the corresponding models were proposed by research, such as classical truss model and strut model Paulay *et al.* (1978). However, most of these models do not consider the crack configuration of T-shaped column structure.

In the current research (Cao *et al.* 1995, Pham *et al.* 2015), the seismic behavior of T-shaped column joints is studied. It is found that the crack formation of the T-shaped frame column joints is different from that of the conventional rectangular column under cyclic loading. For the conventional rectangular column, a cross crack nucleates and propagates along the diagonal of joint, and the crack is X-shaped; the whole joint was divided into 4 portions (respectively, region ①, ②, ③ and ④) by diagonal crack as shown in Fig. 6(a).

The cracks of the T-shaped column joints show the reversed K-shaped failure mode which is also divided into 4 portions (region ①, ②, ③ and ④, respectively) by the crack, as in Fig. 6(b). However, compared with the conventional joint, the flange of T-shaped column is equivalent to fixing the end of region ② and provides stronger restraint to region ②. Furthermore, the beam provides weak restraint to region ④ because of the relatively tiny stiffness of beam. Hence, region ④ is invaded by region ②, with the expansion of region ②, the range of region ④ will shrink gradually, and the cross point of X-shaped crack moves to the beam end, and the X-
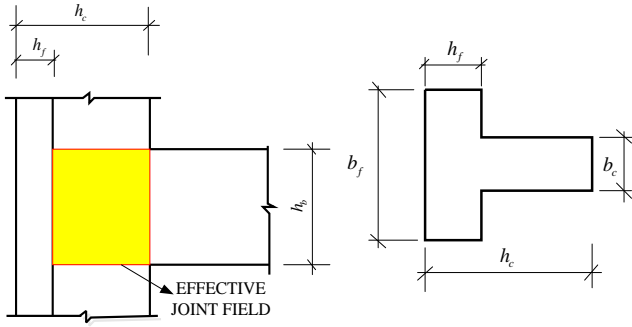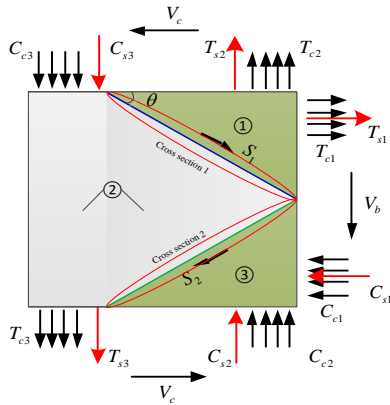
Fig. 7 The effective range of T shape column joint

shaped crack is eventually transferred into the reversed K-shaped crack.

The experiment shows that the cracks mainly occurred in the web of the T-shaped column joints under cyclic loading. Therefore, we assumed that the width of the joint is equivalent to the width of the T-shape column, and the flange of T-shaped column is regarded as the enhanced part, as shown in Fig. 7. The height of the joint is equivalent to the beam section height, and the thickness of joint is equal to the average thickness of column web.

Based on the plastic hinge failure mechanism, the tensile-shear failure model of T-shaped column joints under cyclic loading is proposed, as shown in Fig. 8, and the joint area is composed of three parts in this model. Where region ① will be stripped from joint area along the direction of load $T_{s1}$, and when the value of $T_{s1}$ reaches a critical value, cracks will emerge along the cross section 1. With the value of $T_{s1}$ increasing gradually, the fracture surface is formed along cross section 1. Region ② consists of the flange and web of T-shaped column. Analogously, region ② has a tendency to squeeze in the internal joints under the action of $C_{s1}$. If the stress along the cross section 2 exceeds the shear bearing capacity, cracks will be formed. When the load is reversed, the stress state of region ① and ② is opposite. Hanson *et al.* (1967) reported that the shear of joints is caused by the horizontal force acted at the mid-height of the

joints. The form of shear is shown in Fig. 9, when shear acts on the exterior edge of joint, the status of joint is identical to the vertical beam, as shown in Fig. 9. Region ① and part of region ② are deemed as a whole, which is damaged in virtue of the fracture caused by region ① in tension. This form of failure is inclined to be diagonal tension failure. The whole region constituted by region ③ and part of region ② under shear may subject to diagonal tension failure, shear-compression failure, and diagonal tension failure due to the difference between T-shaped column web thickness and beam height. The concept of shear span ratio of joints is introduced to analyze the failure model of the joint.

In the current research, the shear failure patterns of the joints are analyzed, the contribution of reinforcements and concrete to the shear capacity of the joint is considered by

$$V_j = T_s + T_c - V_c \tag{4}$$

where $V_j$ is shear of joint; $T_s$ is tension of the reinforcement; $T_c$ is tension of the concrete.

At the interface of the beam and column, as shown in Fig. 9, the tension can be obtained from the compressive zone of joint:

$$T_s + T_c = \frac{M_b}{h_j} \tag{5}$$

where $M_b$ is the moment of beam end.

According to the relationship between $F_b$ and $V_b$ with respect to the moment of contraflexure point:

$$V_c = \frac{F_b l_b}{l_c} \tag{6}$$

where $F_b$ is the loads applied at the loading point; $L_b$ is the vertical distance from the loading point on the beam end to the column center; and $l_c$ is the distance between two contraflexure points of T-shaped column.

Under the action of load $F_b$ of the free end of a beam, the moment at the junction of beam and column $M_b=F_b l_b$, and $M_b=\Sigma M_c$ can be obtained according to the moment





*Note: $T_{si}$, $C_{si}$ represents the tension and compression of reinforcement respectively; $T_{ci}$, $C_{ci}$ represents the tension and compression of concrete respectively; $V_c$ is the shear of T-shaped column; $V_b$ is the shear of beam; $h_j$ represents the distance between tension and compression on cross section at beam end.

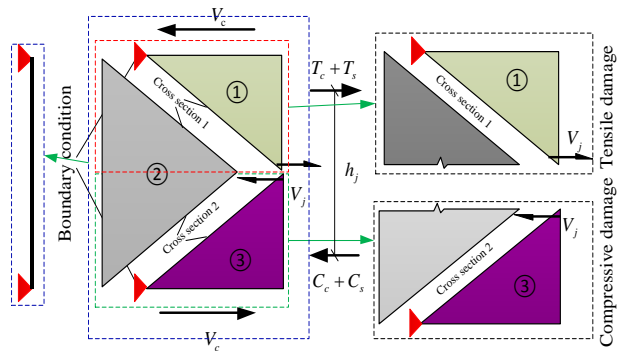Fig. 8 Failure model of joint                    Fig. 9 Schematic of joint decomposition

equilibrium of joints. Substituting Eqs. (5)-(6) into Eq. (4) gives

$$V_j = \frac{M_b}{h_j} - \frac{M_b}{l_c} = \frac{M_b(l_c - h_j)}{l_c h_j} \qquad (7)$$

The normal stress of joint is

$$\sigma = \alpha_1 \frac{M_b}{b_c(h_c - h_f - a_{sc})^2} \qquad (8)$$

The shear stress in the joint is

$$\tau = \alpha_2 \frac{M_b(l_c - h_j)}{h_j l_c b_b(h_c - h_f - a_{sc})} \qquad (9)$$

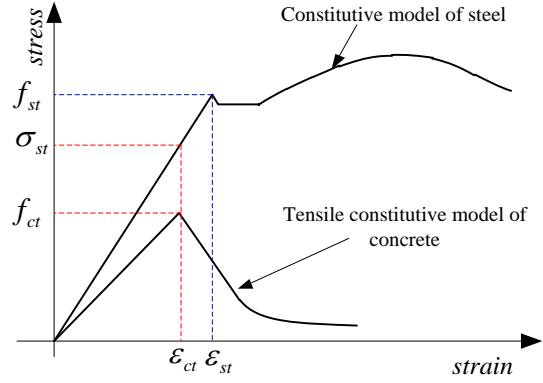The ratio of normal stress and shear stress can be calculated by

$$\frac{\sigma}{\tau} = \frac{\alpha_1}{\alpha_2} \frac{h_j l_c}{(h_c - h_f - a_{sc})(l_c - h_j)} \qquad (10)$$

Consequently, the shear span ratio of joint is defined as

$$\lambda = \frac{h_j l_c}{(h_c - h_f - a_{sc})(l_c - h_j)} \qquad (11)$$

where $\alpha_1$ and $\alpha_2$ are constant; and $\alpha_{sc}$ is the distance between the resultant of the longitudinal reinforcements in the compression zone to the column edge. The shear span ratio $\lambda$ is adopted to assess the failure pattern of the joint. Here, the joint is divided into two parts according to the joint shear force: the tensile region and the compressive region. The compressive zone is shown in Fig. 8; Eq. (11) and shows that only when T-shaped column web is greater than $(1.2-1.5)h_j$, the shear span ratio $\lambda<1$. At this moment, the joints exhibit horizontal diagonal compressive failure. Although the joint bearing capacity of this damage pattern is large, the failure is brittle failure and does large damage to the structure, especially in moderate and large earthquakes. Since the section height of beam cannot exceed height of column, $\lambda>3$ will not occur. Generally, the shear span ratio of joint is $1\leq\lambda\leq3$, and then the joints will show horizontal compressive-shear failure. Notwithstanding that this failure form is brittle failure, its ductility is superior compared with other types of failure. Similarly, when the joint shear span ratio in the tension zone conforms to $\lambda<1$, diagonal tensile failure damage of the joints arises. When the joints shear span $1\leq\lambda\leq3$, the joint has the tensile-shear failure.

The joint failure model is based on the classical truss and strut mechanism and views the yield of stirrup or compression failure of concrete as a sign of joint failure (Shiohara 2001). However, the reinforcements and concrete at the fracture zone cannot reach the yield simultaneously because of different deformation capacities. Under the circumstances that ensuring the bend capacity of the joint zone, reinforcement strain and concrete strain of joint are coordinated in the shear initial stage. With increasing strain at the joint core zone, concrete reaches the ultimate strain but the reinforcements do not reach the yield strength, which is due to the fact that reinforcement has a stronger deformation capacity, as shown in Fig. 10. Therefore, it is



*Note: $\varepsilon_{ct}$ is the ultimate tensile strain of concrete, $\varepsilon_{st}$ is the tensile yield strain of reinforcement, $f_{ct}$ is the ultimate tensile strength of concrete, $f_{st}$ is tensile yield strength of reinforcement, $\sigma_{st}$ is tensile strength of reinforcement corresponding to the concrete yield strain, $a_{sb}$ is protective layer thickness of concrete beams, $a_{sc}$ is protective layer thickness of concrete columns.

Fig. 10 Comparison of stress-strain of reinforcement and concrete

inappropriate to regard the single index as a joint failure of reinforcement and concrete. Calculating the shear bearing capacity of joints requires a comprehensive consideration of both factors, and the maximum value as the index of joint shear bearing capacity can be calculated by comparing these two indicators.

Experimental and theoretical analysis show that tensile failure is present in the tensile zone; and compressive failure is present in the compressive zone under vertical load. Due to the bearing capacity of compressive shear failure being higher than the tensile-shear failure, joints show mainly tensile shear failure in the tensile zone under cyclic loading. The critical shear resulting in failure of joints is divided into two cases, because the ultimate strain of concrete and reinforcement of joint is uncoordinated, as shown in Fig. 10: (i) the shear bearing force of joint depends on the ultimate crack bearing capacity of core concrete in joint and tension of transverse reinforced corresponding to cracking strain of concrete. Instead, the sign of shear failure is forming a crack that penetrates the whole joint, which occurs in the limit stage of stirrup and concrete working together. In this failure, the transverse reinforcements bearing capacity is less than the shear bearing capacity of joints; hence, after the joint concrete failure, the joint is immediately destroyed. In practice, design engineers should avoid the brittle failure caused by the high strength of concrete in the joint. (ii) the shear bearing force of joint depends on the yield strength of stirrup in joint. A sign of joint failure is the tensile failure of transverse reinforcements intersected with crack. After joint concrete failure, the joint bearing capacity does not reach the maximum value, the stirrups carrying shear; therefore the contribution of the transverse stirrups are only considered in the calculation of the joint bearing capacity and the dowel action of other reinforcements is neglected, and this failure pattern has good ductility. By neglecting the axial compression ratio effect, the shear bearing capacity $V_R$

can be obtained from two kinds of calculation formulas.

Based on the failure model, the maximum shear bearing capacity that is provided by the concrete of the fracture section in the joint zone (such as in Fig. 9 cross Section1) is equivalent to the product of the diagonal fracture surface area of internal core concrete and the tensile strength of concrete

$$V_c = \frac{h_c - h_f - a_{sc}}{\cos\theta} f_t (b_c - 2a_{sb}) \tag{12}$$

where $\theta$ is the intersection angle between the fracture surface and the horizontal axis, as shown in Fig. 8. When the angle increases (i.e., the inclined angle of section1 cross increases), the shear bearing capacity of concrete will be increased, as shown in Fig. 9. Moreover, the shear strength of joints will be increased as well. In order to improve the safety of joints, the unfavorable damage position is chosen as shown in Fig. 8. Therefore, the value of $\theta$ can be

obtained: $\theta = \arctan \dfrac{h_b}{2(h_c - h_f - a_{sc})}$.

According to the crack form of the joints, the opinion that the shear bearing force of joints contributed by the transverse stirrups in the joint is divided into two parts. The transverse stirrups in the tensile zone are mainly subject to tension, while the transverse stirrups in the compression zone mainly subject to compression. Due to the joints showing mainly tensile-shear failure, the stirrups in the tensile zone of the joints play a decisive role. Therefore, the maximum shear bearing capacity of the transverse stirrups is defined as

$$V_s = f_{yv} A_s \left\lfloor \frac{h_b - 2a_{sb}}{2s} \right\rfloor \tag{13}$$

where $f_{yv}$ is the tensile strength of transverse stirrups of joint; $A_s$ is stirrup area of the transverse section of joint; $a_{sb}$ is protective layer thickness of beams; $s$ is instance of stirrups in the joint zone; $\lfloor x \rfloor$ is mathematical symbol and the value is an integer not larger than $x$.

When the joints are subjected to shear forces, the reinforcements and concrete cannot reach the tensile yield simultaneously because of different deformation capacities. Therefore, this case is divided into two stages when the joints are subjected to shear forces: one is the stage of concrete and reinforcement co-working in joints. The largest shear bearing capability of joints emerges at the critical state of failure of core concrete in the joint. At the same time, the core concrete has reached the ultimate cracking bearing capacity, while the transverse stirrups in this strain are still in elastic stage. The formula for calculating the shear capacity of the joint is

$$V_c + V_s = V_c + V_s = (h_c - h_f - a_{sc})(b_c - 2a_{sc}) f_{ct}$$
$$+ \sigma_{st} A_s \left\lfloor \frac{h_c - h_f - a_{sb}}{s} \right\rfloor \tag{14}$$

where $\sigma_{st}$ is the tensile strength of the reinforcements, corresponding to the tensile cracking strain of concrete; and $a_{sc}$ is the thickness of the protective layer for the column.

When the shear strength provided by the transverse stirrups of joints is greater than the values calculated by Eq. (14), the shear strength of joint depends on the yield strength of the stirrups after concrete cracking. It is the sign of the joint's failure that the transverse stirrups yield in the fracture zone and the shear resistance capacity are obtained by calculating Eq. (13). Since the concrete in the core zone does not contribute to the shear bearing capacity after cracking, the shear bearing capacity equals the product of shear strength and the area of transverse stirrups. Therefore, when calculating the ultimate bearing capacity of joints, the calculation formulas of the above two cases should be compared, and the maximum value is the index of shear bearing capacity of the T-shaped column joints.

Therefore, the shear capacity of T-shaped column joints can be obtained

$$V_R = MAX \left( (h_c - h_f - a_{sc}) f_{ct}(b_c - 2a_{sb}) \right.$$
$$\left. + \sigma_{st} A_s \left\lfloor \frac{h_c - h_f - a_{sc}}{s} \right\rfloor, \ f_{yv} A_s \left\lfloor \frac{h_b - 2a_{sb}}{2s} \right\rfloor \right) \tag{15}$$

It is essential to predict accurately the shear resistance of the joints, which has a great influence on preventing the occurrence of shear hinge and determining the location of the plastic hinge.

## 5. Conclusions

From the experimental and theoretical analysis to 6 frame joints of T-shaped reinforced concrete special shaped column, the following conclusions can be drawn:

• With increasing of the beam section height, the bearing capacity of the T-shaped column increases profoundly. The improvement of bearing capacity is mainly from the contribution of section change. Due to the failure of the beam hinge, increase of axial pressure ratio and joint transverse stirrup ratio has negligible effect to the capacity of T-shaped side column.

• It is experimentally observed that the crack is formed in the reversed "K" mode in the core concrete. The interaction point of X-shaped crack in the conventional rectangular joint moves towards the outside of the joint, and extends to both ends in vertical direction, which eventually forms the reversed K-shaped crack.

• Based on the experimental observations of the cracks, a tensile-shear failure model for T-shaped column joint is proposed. The failure pattern is predicted by employing the shear span ratio to the joint analysis, and the failure mechanisms of joints are described. A theoretical model to predict the shear bearing capacity of the joint is developed, which shows reasonable accuracy compared with experimental results.

## References

ACI 318R-08 (2014), Building Code Requirements for Structural Concrete and Commentary, American Concrete Institute, Farmington Hills, MI, USA

Bakir, P. and Boduroğlu, H. (2002), "A new design equation for predicting the joint shear strength of monotonically loaded exterior beam-column joints", *Eng. Struct.*, **24**(8), 1105-17.

Barbhuiya, S. and Choudhury, A.M. (2015), "A study on the size effect of RC beam-column connections under cyclic loading", *Eng. Struct.*, **95**, 1-7.

Behnam, H., Kuang, J.S. and Huang, R.Y.C. (2017), "Exterior RC wide beam-column connections: Effect of beam width ratio on seismic behavior", *Eng. Struct.*, **147**, 27-44.

Bossio, A., Fabbrocino, F. and Lignola, G.P. (2015), "Simplified model for strengthening design of beam-column internal joints in reinforced concrete frames", *Polym. Basel*, **7**(9), 1732-1754.

Cao, W.L., W, G.Y. and Wei, W.X. (1995), "Behavior of T-shaped column under different directional cyclic loading", *Earthq. Eng. Eng. Vib.*, **15**(4), 76-84.

Chen, C.H., Zhu, Y.F., Yao, Y. and Huang, Y. (2016), "Progressive collapse analysis of steel frame structure based on the energy principle", *Steel Compos. Struct.*, **21**(3), 553-71.

Chen, C.H., Zhu, Y.F., Yao, Y., Huang, Y. and Long, X. (2016), "An evaluation method to predict progressive collapse resistance of steel frame structures", *J. Constr. Steel Res.*, **122**, 238-50.

Dundar, C. and Sahin, B. (1993), "Arbitrarily shaped reinforced concrete members subject to biaxial bending and axial load", *Comput. Struct.*, **49**(4), 643-62.

Euro Code 8 (2004), Design of Structures for Earthquake Resistance. Part 1: General Rules, Seismic Actions and Rules for Buildings, London, UK.

Ghobarah, A. and Said, A. (2002), "Shear strengthening of beam-column joints", *Eng. Struct.*, **24**(7), 881-8.

Gosain, N.K., Brown, R.H. and Jersa, J. (1977), "Shear requirements for load reversals on RC members", *J. Struct. Div.*, **103**(7), 1461-1476.

Hanson, N.W. and Conner, H.W. (1967), "Seismic resistance of reinforced concrete beam-column joints", *J. Struct. Div.*, **93**(5), 533-60.

Hwang, S.J. and Lee, H.J. (2000), "Analytical model for predicting shear strengths of interior reinforced concrete beam-column joints for seismic resistance", *ACI Struct. J.*, **97**(1), 35-44.

Hwang, S.J., Lee, H.J., Liao, T.F., Wang, K.C. and Tsai, H.H. (2005), "Role of hoops on shear strength of reinforced concrete beam-column joints", *ACI Struct. J.*, **102**(3), 445-53.

Jeon, J.S., Shafieezadeh, A. and DesRoches, R. (2014), "Statistical models for shear strength of RC beam-column joints using machine-learning techniques", *Earthq. Eng. Struct. D.*, **43**(14), 2075-95.

Kim, J. and LaFave, J.M. (2007), "Key influence parameters for the joint shear behaviour of reinforced concrete (RC) beam-column connections", *Eng. Struct.*, **29**(10), 2523-39.

Kim, J. and LaFave, J.M. (2009), "Joint shear behavior of reinforced concrete beam-column connections subjected to seismic lateral loading", Newmark Structural Engineering Laboratory. University of Illinois at Urbana-Champaign.

Kitayama, K., Otani, S. and Aoyama, H. (1988), "Earthquake resistant design criteria for reinforced concrete interior beam-column joints", *Tran. JCI.*, **10**, 281-8.

LaFave, J.M. and Kim, J.H. (2011), "Joint shear behavior prediction for RC beam-column connections", *Int. J. Concr. Struct. M.*, **5**(1), 57-64.

Lee, J.Y., Kim, J.Y. and Oh, G.J. (2009), "Strength deterioration of reinforced concrete beam-column joints subjected to cyclic loading", *Eng. Struct.*, **31**(9), 2070-85.

Li, S. F., Li, Q. N. and Zhang, H. (2018), "Experimental study of a fabricated confined concrete beam-to-column connection with end-plates", *Constr. Build. Mater.*, **158**, 208-216.

Masi, A., Santarsiero, G., Lignola, G.P. and Verderame, G.M. (2013), "Study of the seismic behavior of external RC beam-column joints through experimental tests and numerical simulations", *Eng. Struct.*, **52**, 207-19.

Mitra, N. and Lowes, L.N. (2007), "Evaluation, calibration, and verification of a reinforced concrete beam-column joint model", *J. Struct. Eng.*, **133**(1), 105-20.

NZS 3101(2006), Concrete Structures Standard. Part 1: The Design of Concrete Structures, Standard Association of New Zealand (SANZ), Wellington, New Zealand.

Park, S. and Mosalam, K.M. (2012), "Parameters for shear strength prediction of exterior beam-column joints without transverse reinforcement", *Eng. Struct.*, **36**, 198-209.

Paulay, T., Park, R. and Preistley, M. (1978), "Reinforced concrete beam-column joints under seismic actions", *ACI J.*, **75**(11), 585-93.

Pham, T.P. and Li, B. (2015), "Seismic performance assessment of L-shaped reinforced concrete columns", *ACI Struct. J.*, **112**(6), 667.

Ricci, P., Maria, D.R.M., Verderame, G.M. and Manfredi, G. (2016), "Experimental tests of unreinforced exterior beam-column joints with plain bars", *Eng. Struct.*, **118**, 178-94.

Scott, R. (1992), "The effects of detailing on RC beam/column connection behaviour", *Struct. Eng.*, **70**(18), 318-24.

Shiohara, H. (2001), "New model for shear failure of RC interior beam-column connections", *J. Struct. Eng.*, **127**(2), 152-60.

Tsonos, A.G. (2007), "Cyclic load behavior of reinforced concrete beam-column subassemblages of modern structures", *ACI Struct. J.*, **104**(4), 468.

Unal, M. and Burak, B. (2012), "Joint shear strength prediction for reinforced concrete beam-to-column connections", *Struct. Eng. Mech.*, **41**(3), 421-40.

Wang, G.L., Dai, J.G. and Teng, J. (2012), "Shear strength model for RC beam-column joints under seismic loading", *Eng. Struct.*, **40**, 350-60.

Wong, H. and Kuang, J.S. (2008), "Effects of beam-column depth ratio on joint seismic behaviour", *P I Civil Eng. Struct. B.*, **161**(2), 91-101.

*CC*